Breaking the resolution limit for acoustic imaging using positivity and sparsity

Georg Watzl, Edgar Scherleitner, Peter Burgholzer

Breaking the resolution limit for acoustic imaging using positivity and sparsity

Georg Watzl[1] **Edgar Scherleitner**[1] **Peter Burgholzer**[1]
[1] Research Center for Non-Destructive Testing (RECENDT), 4040 Linz, Austria
georg.watzl@recendt.at

ABSTRACT

Ultrasound imaging through tissue suffers from a loss of image quality with increasing layer thickness, which is mostly due to acoustic attenuation, including absorption and scattering. The reconstruction of a propagated wave form to the shape as it would have been without attenuation is an ill-posed inverse mathematical problem. This is due to the second law of thermodynamics, which states, that dissipative processes, such as sound absorption, are not reversible, leading to a loss of information. This information is strongly related to the achievable resolution in acoustic imaging. In a power-law attenuation model higher frequency components experience higher damping than the low frequency portions of the wave leading to a broadening of the initial pulse.

In this work we are presenting a new method to overcome these limitations for piezoelectric ultrasound in biological media utilizing positivity and sparsity constraints for the inversion within a Douglas-Rachford regularization schema. This requires accurate knowledge of the frequency dependent acoustic attenuation in the medium. Reference measurements in a medium with negligible attenuation, such as water, allows the incorporation of the measurements systems transmit and receive characteristics. The method is demonstrated experimentally with A-Mode piezoelectric through-transmission measurements in liquids. For a first demonstration glycerol as a liquid with rather high viscosity and therefore high acoustic attenuation is used – approximately 100 times higher than in water.

1. INTRODUCTION

Super resolution acoustic imaging has been previously shown by Burgholzer et al. in photoacoustic imaging with external broad-band plane wave laser-ultrasonic excitation and a coaxial piezoelectric receiver [1]. The same principles can be applied to ultrasonic plane waves generated by piezoelectric array transducers.

The received attenuated pressure as a function of time at an axial distance of z from the transmitting transducer array ($\boldsymbol{p}$) can be described by an algebraic equation system.

$$\boldsymbol{p} = \boldsymbol{M}_z \boldsymbol{M}_\mathrm{s} \boldsymbol{p}_\mathrm{i} \tag{1}$$

$\boldsymbol{M}_z$ is the acoustic attenuation tensor, $\boldsymbol{M}_\mathrm{s}$ describes the systems input response and receive characteristics and $\boldsymbol{p}_\mathrm{i}$ is a short pulse excitation, ideally a Dirac delta pulse. Combining the ultrasound system response and the description of the wave propagation in one matrix $\boldsymbol{M} = \boldsymbol{M}_z \boldsymbol{M}_\mathrm{s}$ allows to use sparsity and positivity assumptions for the reconstruction of the ideal pressure signal $\boldsymbol{p}_\mathrm{i}$ from the measured $\boldsymbol{p}_z$. This inversion of Eq. 1 is an ill-posed or ill-conditioned inverse problem. The spatial resolution degrades with increasing depth because higher acoustic frequencies, which have smaller wavelengths and allow a better resolution, are stronger attenuated than lower frequencies. Although acoustic attenuation defines the ultimate spatial resolution limit, other factors such as detector bandwidth, element size and the transmission and detection aperture can be additional limiting factors. Mathematically, the ill-posed inverse problem needs regularization to achieve stable solutions. Classically, the requirement of the smoothness of the solution is often used for regularization, which can be described in frequency domain by limiting the highest frequencies in the signal by a cut-off frequency ω_cut. The spatial resolution limit according to Nyquist is half the wavelength at this frequency

$$\delta_\mathrm{resolution} = \frac{\pi}{\omega_\mathrm{cut}} c, \tag{2}$$

with the sound velocity c. For a plane wave, a Dirac's delta pulse δ after travelling a distance z in a liquid, such as water or glycerol, the pressure p can be described as (e.g. [2])

$$p(z,t) = \frac{1}{2\pi}\sqrt{\frac{\pi}{\alpha_0 z}} \exp\left(-\frac{(z/c - t)^2}{4\alpha_0 z}\right), \tag{3}$$

where α_0 is the attenuation constant, and t the time. According to [2], for a one-dimensional plane wave a relationship between the non-attenuated plane wave p_i and the attenuated wave p can be established:

$$p(z,t) = p_i(z,t) \star \frac{1}{2\pi}\sqrt{\frac{\pi}{\alpha_0 z}} \exp\left(-\frac{t^2}{4\alpha_0 z}\right), \tag{4}$$

where $\star$ denotes the time convolution, which is in vector notation the multiplication by $\boldsymbol{M}_z$ in Eq. (1).

In the frequency domain, acoustic attenuation in water is described by a power-law dependence, as can be seen by the Fourier transformation of Eq. (3):

$$\tilde{p}(z,\omega) = \int_{-\infty}^{\infty} p(z,t)\exp(i\omega t)\,\mathrm{d}t = \exp\left(i\omega\frac{z}{c}\right)\exp(-\alpha_0\omega^2 r), \tag{5}$$

where the Fourier transformation of the time convolution is the product of the Fourier transformations. Acoustic attenuation in a liquid is proportional to the square of the frequency ω. The Kramers-Kronig relationship states that for a power-law with an exponent of two there is no dispersion, and therefore the sound velocity c does not depend on the frequency ω.

2. EXPERIMENTAL SETUP

A custom 128 element linear array ultrasound transducer (Imasonic®) is coaxially aligned with a single piston-shaped immersion transducer (NDTSystems®). The array transducer is driven by the Verasonics® Vantage 64 research ultrasound system. A front plate adapter was built in-house to be able to connect the 160 pin Hypertronics® type plugs of the ultrasonic array probes to the multiplexed 260 pin ZIF (zero insertion force) socket, which is installed on the Vantage 64 system (Figure 1).

The validity of this approach requires $\boldsymbol{M}_s$ to be constant over the whole measurement range, which implies plane wave conditions. The finite aperture of the source pulse generating transducer and the spacing between single transducer elements in the array creates complex refraction patterns in the sound field. Therefore, a region with approximate plane wave conditions must be identified.

To this end the measurement setup was digitally modelled using the k-Wave toolbox developed by Treeby et al. [3]. The resulting cross-section image, which is included as background of the measurement path in Figure 1, indicates plane wave conditions after a propagation length of around 5 mm. The side lobes limit the maximal off-axis distance to around 12 mm within the simulated propagation distance range of 30 mm.

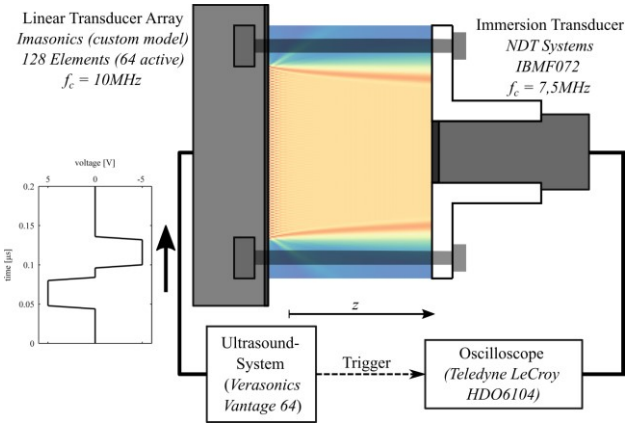

Figure 1. Measurement set-up. Signals were acquired at a distance 5, 10, 15, 20, 25 and 30 mm. $z = 0$ was chosen at a depth of 5 mm to guarantee plane wave conditions.

3. RESULTS

To be sure to have plane wave conditions $z = 0$ was chosen to be at a depth of 5 mm. Further measurements were made at $z = 5, 10, 15, 20$ and 25 mm. The signals are shown in Figure 3. 10 measurements were averaged for each distance to get a better signal-to-noise ratio. The time scale was shifted for each signal to allow plotting all the signals in the same plot.

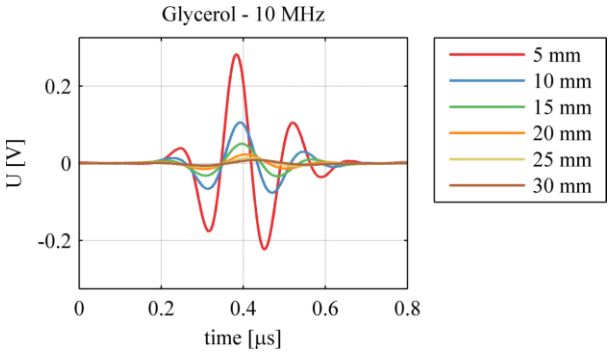

Figure 2. Measured time-shifted ultrasound waveforms in glycerol at acoustic path lengths from 5 mm to 30 mm ($\boldsymbol{p}$) acquired with the through-transmission setup shown in Figure 1.

By Fourier transformation in time the amplitude in frequency domain for the signals was calculated (Figure 4). The acoustic attenuation coefficient in dB was determined by

$$\alpha(\omega)z = -20\log(|\tilde{p}(z,\omega)|/|\widetilde{p_{\text{ideal}}}(z,\omega)|), \qquad (6)$$

Where log is the logarithm to base 10. It turns out that a power law

$$\alpha(\omega) = \alpha_0|\omega|^n, \qquad (7)$$

with an exponent $n = 2$ and $\alpha_0 = 0.4\ dB\ MHz^{-2}\ cm^{-1}$ fits the attenuation in a wide frequency range very well. Above the cut-off frequency ω_{cut}, which decreases with propagation distance, the signal amplitude gets lower than the noise level and the attenuation cannot be determined any more.

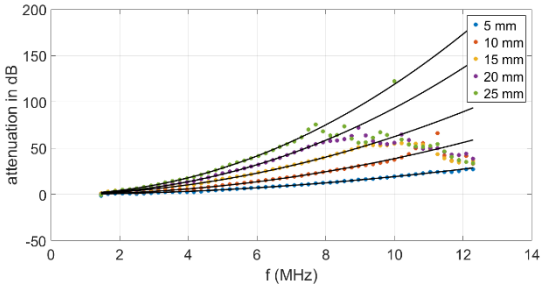

Figure 3. Acoustic attenuation at a propagation distance of $z = 5, 10, 15, 20,$ and 25 mm shown as dots. The black lines indicate the attenuation given by the power-law in Eq. 6. This adequately describes the acoustic attenuation for the propagation in glycerol.

Using these measured signals, Eq. (1) is now inverted by truncated singular value decomposition (T-SVD) [4], which allows negative values and does not enforce sparsity (Figure 4). The matrix $\boldsymbol{M}_s$ is given by the measurement signal at $z = 0$ and the matrix $\boldsymbol{M}_z$ is the time convolution as shown in Eq. (4).

The second method for the inversion of Eq. (1) is the Douglas Rachford splitting algorithms (DR algorithm), which uses positivity and sparsity of the ideal signal $\boldsymbol{p}_i$ [5-6]. This algorithm allows a better resolution than half of the wavelength at the truncation frequency, as given in Eq. (2) (Figure 5). This resolution enhancement is demonstrated in 1D here, but the same resolution enhancement is expected in axial direction in 3D by using spherical projection. In lateral direction the resolution enhancement might be less, due to limited angle effects.

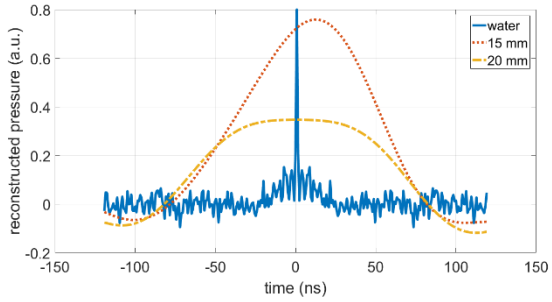

Figure 4. Reconstruction results using T-SVD for regularization to compensate attenuation after 15 mm (red dotted line) and 20 mm (yellow dashed line) propagation in glycerol. The matrix $\boldsymbol{M}_z$ was multiplied by the convolution matrix of the water signal to get a positive δ - like pulse for the $z = 0$ signal (blue solid line).

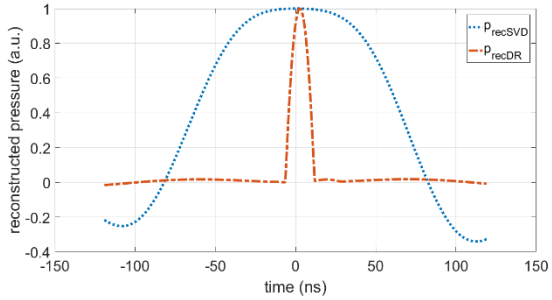

Figure 5. Compensation of acoustic attenuation after 20 mm propagation in glycerol: T-SVD (blue dotted line. FWHM of 120 ns), and DR method (red dashed dotted and line) with 60 iterations (FWHM of 13 ns). For the linear SVD reconstruction the width of the peak gives the spatial resolution, for the DR method, this is not necessarily the case. The signals are normalized to have a maximum of one.

4. DISCUSSION AND OUTLOOK

Especially in fatty tissue the acoustic attenuation limits the resolution in ultrasound imaging. Compensation of acoustic attenuation is an ill-posed inverse problem. Using sparsity and positivity of the signals allows iterative non-linear reconstruction methods for regularization. This gets possible by combining the pulse response of the ultrasound system (transducers, signal processing etc.) with the propagation matrix due to acoustic attenuation. Solving this together gives a significant increase in resolution.

For a quantification of the resolution enhancement the imaging of small steps could help, as for a nonlinear reconstruction method the peak width, e.g. the full-width-at-half-maximum (FWHM) is not directly related to the spatial resolution, as it is the case for linear reconstruction methods. This is planned for future work.

5. ACKNOWLEDGMENT

Measurements were funded by the project “multimodal and in-situ characterization of inhomogeneous materials” (MiCi) by the federal government of Upper Austria and the European Regional Development Fund (EFRE) in the framework of the EU-program IWB2020. Signal and data processing was also funded within the strategic economic-research program “Innovative Upper Austria 2020” of the province of Upper Austria. Parts of this work have been supported by the Austrian Science Fund (FWF), projects P 30747-N32 and P 33019-N.

6. REFERENCES

[1] P. Burgholzer, J. Bauer-Marschallinger, and M. Haltmeier, “Breaking the resolution limit in photoacoustic imaging using non-negativity and sparsity,” *Photoacoustics*, vol. 19, no. March, p. 100191, 2020, doi: 10.1016/j.pacs.2020.100191.

[2] X. L. Den-Ben, D. Razansky, and V. Ntziachristos, “The effects of acoustic attenuation in optoacoustic signals,” *Phys. Med. Biol.*, vol. 56, no. 18, pp. 6129–6148, 2011, doi: 10.1088/0031-9155/56/18/021.

[3] B. E. Treeby and B. T. Cox, “k-Wave: MATLAB toolbox for the simulation and reconstruction of photoacoustic wave fields,” *J. Biomed. Opt.*, vol. 15, no. 2, p. 021314, 2010, doi: 10.1117/1.3360308.

[4] P. Burgholzer, M. Thor, J. Gruber, and G. Mayr, “Three-dimensional thermographic imaging using a virtual wave concept,” *J. Appl. Phys.*, vol. 121, no. 10, 2017, doi: 10.1063/1.4978010.

[5] J. Eckstein and D. P. Bertsekas, “On the Douglas-Rachford splitting method and the proximal point algorithm for maximal monotone operators,” *Math. Program.*, vol. 55, no. 1–3, pp. 293–318, 1992, doi: 10.1007/BF01581204.

[6] J. Eckstein and W. Yao, “Relative-error approximate versions of Douglas–Rachford splitting and special cases of the ADMM,” *Math. Program.*, vol. 170, no. 2, pp. 417–444, 2018, doi: 10.1007/s10107-017-1160-5.